Nonlinear Dynamics and Systems Theory, **5**(3) (2005) 251–264

Influence of Propellant Burn Pattern on the Attitude Dynamics of a Spinning Rocket

F.O. Eke[1]* and J. Sookgaew[2]

[1] *Department of Mechanical and Aeronautical Engineering, University of California, Davis, CA 95616, USA*

[2] *Department of Mechanical Engineering, Prince of Songkla University, Hatyai, Thailand*

Received: May 16, 2005; Revised: June 15, 2005

Abstract: This study examines the effect of various propellant burn geometries on the attitude dynamics of a rocket-type variable mass system. The three burn scenarios studied are the end burn, the centripetal burn, and the radial burn. Results of this study indicate that a change in burn scenario changes the predicted attitude motion. The differences are more pronounced for spin motion than for transverse attitude motion. The end burn is recommended whenever it is practically feasible; it is found to be the least disruptive from the point of view of attitude dynamics.

Keywords: *Rockets; variable mass systems; attitude dynamics.*

Mathematics Subject Classification (2000): 70P05, 70M20, 34C60.

1 Introduction

In the study of the dynamics of rockets, the fact that the system undergoes substantial mass variation is generally captured in one of two ways. One method is to view the system as a solid whose mass and inertia vary as functions of time [4, 5]. The exact time functions used for both the mass and inertia scalars are based on reasonable guesses of what is likely to occur in real systems. Another approach is to show the propellant as a subsystem of the rocket, and then specify the physical and geometric manner in which the propellant mass is depleted. These facts are then used for the precise calculation of the mass and inertia functions for the system. Naturally, the second approach is preferable, since it eliminates the need for guessing the time histories of the mass/inertia properties. However, authors that have utilized this second approach have generally used very simple

*Corresponding author: foeke@ucdavis.edu

models for both the rocket system and the propellant [2, 3]. When a more complex model has been used [6], only one propellant burn pattern – the radial burn – is examined. The radial burn assumes that a cylindrically shaped solid propellant is ignited on its axis, and burns radially outwards towards its periphery. Yet, there are situations where it makes sense to assume an end burn for example; that is, a burn in which a cylindrical propellant is ignited at one of its ends, and burns towards the opposite end.

The goal of this paper is to examine if and how a change in burn pattern influences predictions of the attitude behavior of a rocket system. Specifically, three different burn patterns will be compared: the end burn, the centripetal burn, and the radial burn. This is important for two reasons. First, this study will lead to reasonably accurate predictions for a case that is in fact best captured by one of the burn scenarios studied, and for which results were previously unavailable. The second reason is that the results can be used as design tool in determining the type of propellant burn that should be implemented in order to produce certain desired dynamic effects.

2 Equations of Attitude Motion

The system studied here is a solid rocket motor and its payload, shown schematically in Figure 2.1. B represents the rocket's main body, assumed rigid, and F is the solid fuel. The products of combustion are expelled through the nozzle. Both B and F are assumed to be axisymmetric, with a common axis z, and F burns so as to remain axisymmetric at all times. The mass centers F^* of F, B^* of B, and S^* of the overall system S all lie on the axis z. Furthermore, we assume that the motion of the gas products of combustion relative to the rocket body is either axial, or symmetric with respect to the z-axis and with no transverse component. Finally, for this study, the velocity distribution of the exhaust gas particles as they traverse the nozzle exit plane is taken to be uniform as shown in Figure 2.1. The equations of attitude motion for this system can be written in the form (see, for example, [1, 6]):

$$I\dot{\omega}_1 + \left[\dot{I} - \dot{m}\left(z_e^2 + \frac{R_1^2}{4}\right)\right]\omega_1 + [(J-I)\omega_3]\omega_2 = 0, \tag{1}$$

$$I\dot{\omega}_2 + \left[\dot{I} - \dot{m}\left(z_e^2 + \frac{R_1^2}{4}\right)\right]\omega_2 - [(J-I)\omega_3]\omega_1 = 0, \tag{2}$$

$$J\dot{\omega}_3 + \left(\dot{J} - \dot{m}\,\frac{R_1^2}{2}\right)\omega_3 = 0, \tag{3}$$

where J and I are the system's overall central axial and transverse moments of inertia respectively, m is the mass, ω_i $(i = 1, 2, 3)$ are the components of the inertial angular velocity of B in the $\boldsymbol{b}_1$, $\boldsymbol{b}_2$, $\boldsymbol{b}_3$ directions (see Figure 2.1), R_1 is the radius of the nozzle at the exit plane, and z_e is the distance from the overall system mass center, S^*, to the nozzle exit plane.

In order to generate non-dimensional versions of equations (1) – (3), we introduce

$$m_r = -\dot{m} = \int (\boldsymbol{v} \cdot \boldsymbol{b}_3)\rho\, ds = \pi\rho U R_1^2 \tag{4}$$

and

$$m_F = m_{FO} - m_r t, \tag{5}$$

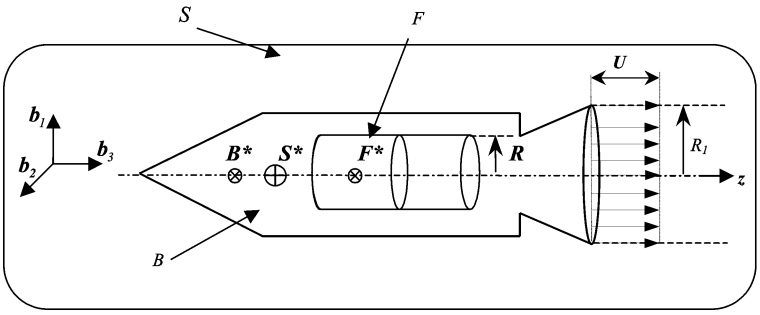

Figure 2.1. Rocket system with solid propellant.

where $\boldsymbol{v}$ is the velocity of exhaust fluid particles relative to the body B, ρ is the mass density of the exhaust gas, m_{FO} is the mass of the solid fuel at ignition, m_F is the instantaneous mass of the fuel, U is the constant magnitude of the axial velocity of the exhaust fluid particles as they cross the nozzle exit plane, and t is time. Hence, the time from ignition to burnout, t_b, is given by

$$t_b = m_{FO}/m_r. \tag{6}$$

Dimensionless time τ, is defined as

$$\tau = t/t_b = (m_r/m_{FO})t. \tag{7}$$

This means that $\tau = 0$ at fuel ignition, and $\tau = 1$ at burnout.

Other useful dimensionless quantities are

$$\bar{m} = m/m_{FO}, \quad \bar{I} = I/m_{FO}R^2, \quad \bar{J} = J/m_{FO}R^2, \quad \text{and} \quad \bar{\omega}_i = \omega_i t_b, \tag{8}$$

where R is the outer radius of the cylindrical propellant grain. Equations (1), (2), and (3) then become respectively

$$\bar{I}\bar{\omega}_1' + \left\{\bar{I}' - \bar{m}'\left[\left(\frac{z_e}{R}\right)^2 + \frac{\beta^2}{4}\right]\right\}\bar{\omega}_1 + [(\bar{J} - \bar{I})\bar{\omega}_3]\bar{\omega}_2 = 0, \tag{9}$$

$$\bar{I}\bar{\omega}_2' + \left\{\bar{I}' - \bar{m}'\left[\left(\frac{z_e}{R}\right)^2 + \frac{\beta^2}{4}\right]\right\}\bar{\omega}_2 - [(\bar{J} - \bar{I})\bar{\omega}_3]\bar{\omega}_1 = 0, \tag{10}$$

and

$$\bar{J}\bar{\omega}_3' + \left(\bar{J}' - \bar{m}'\,\frac{\beta^2}{2}\right)\bar{\omega}_3 = 0. \tag{11}$$

In the above equations, a prime indicates derivative with respect to the dimensionless time variable τ, and β is the nozzle expansion ratio (R_1/R).

From equation (11),

$$\frac{\bar{\omega}_3(\tau)}{\bar{\omega}_3(0)} = \exp\left[-\int_0^\tau \frac{\psi(\tau)}{\bar{J}}\,d\tau\right], \tag{12}$$

where

$$\psi(\tau) = \left(\bar{J}' - \bar{m}' \frac{\beta^2}{2} \right). \tag{13}$$

Next, we follow established tradition [3, 6], and define complex angular velocity

$$\bar{\omega}_T = \bar{\omega}_1 + i\bar{\omega}_2, \tag{14}$$

where $i = \sqrt{-1}$. Equations (9) and (10) are then combined to give

$$\frac{\bar{\omega}_T(\tau)}{\bar{\omega}_T(0)} = \left\langle \exp\left[-\int_0^\tau \frac{\varphi(\tau)}{\bar{J}}\, d\tau \right] \right\rangle \cdot \left\langle \exp\left[i \int_0^\tau \Theta\, d\tau \right] \right\rangle, \tag{15}$$

where

$$\varphi(\tau) = \bar{I}' - \bar{m}' \left[\left(\frac{z_e}{R} \right)^2 + \frac{\beta^2}{4} \right] \tag{16}$$

and

$$\Theta = [(\bar{J}/\bar{I}) - 1]\bar{\omega}_3. \tag{17}$$

It is clear from (15) that the magnitude of the transverse angular velocity vector is controlled by the function $\varphi(\tau)$, while $\Theta(\tau)$ governs the frequency. On the other hand, the sign of $\psi(\tau)$ [see (12)] is an indication of whether the spin rate increases or decreases with τ.

3 Spin Motion

To study the spin rate of the rocket body during propellant burn, it is necessary [see equations (12) and (13)] to determine expressions for instantaneous system mass and inertia. One way to determine these functions is to select a propellant depletion strategy. For this study, we choose to examine three different propellant depletion scenarios: the End Burn, the Centripetal Burn, and the Radial Burn. As the names indicate, End Burn refers to the case where the propellant burns from end to end. Centripetal Burn is the unusual case where propellant burn proceeds radially inwards from the outermost part of the fuel, and Radial Burn is the case where combustion starts from the propellant axis, and proceeds radially outwards.

3.1 End Burn

For the purpose of this study, the solid propellant F is assumed to be a solid cylinder prior to ignition. For the end burn, this cylindrical fuel burns from the end closest to the nozzle towards the opposite end. The burn proceeds uniformly, in the sense that the unburned fuel is always a cylinder of the same radius as at ignition but with diminishing length as shown in Figures 2.1 and 3.1.

Using the symbols defined in Figure 3.1, the mass of fuel F at ignition is

$$m_{FO} = \rho_{FO} \pi R^2 L \tag{18}$$

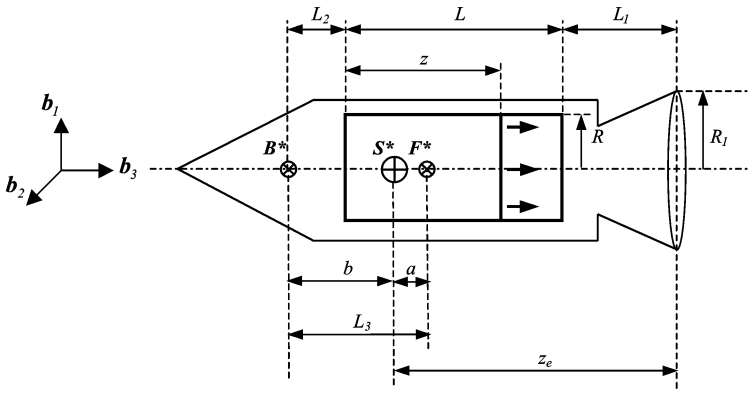

Figure 3.1. Rocket model with end burning propellant.

and the mass at some intermediate stage of the burn is

$$m_F = \rho_{FO}\pi R^2 z, \tag{19}$$

where z is the instantaneous length of the solid cylindrical propellant and ρ_{FO} is its density. From equations (6), (18), and (19), the time from ignition to burnout is

$$t_b = \frac{m_{FO}}{-\dot{m}_F} = \frac{\rho_{FO}\pi R^2 L}{-\rho_{FO}\pi R^2 \dot{z}} = \frac{L}{-\dot{z}}. \tag{20}$$

Integrating (20), we obtain

$$\frac{z}{L} = 1 - \tau. \tag{21}$$

The dimensionless mass of the propellant is

$$\bar{m}_F = \frac{m_F}{m_{FO}} = \frac{\rho_{FO}\pi R^2 z}{\rho_{FO}\pi R^2 L} = \frac{z}{L} = 1 - \tau. \tag{22}$$

Hence,

$$\bar{m}' = \bar{m}'_F = -1. \tag{23}$$

The axial moment of inertia of the propellant is

$$J_F = \frac{m_F R^2}{2} \tag{24}$$

and the dimensionless version is

$$\bar{J}_F = \frac{J_F}{m_{FO}R^2} = \frac{\bar{m}_F}{2} = \frac{1-\tau}{2}. \tag{25}$$

The combined axial moment of inertia of the system is

$$\bar{J} = \bar{J}_B + \bar{J}_F = \bar{J}_B + \frac{(1-\tau)}{2}, \tag{26}$$

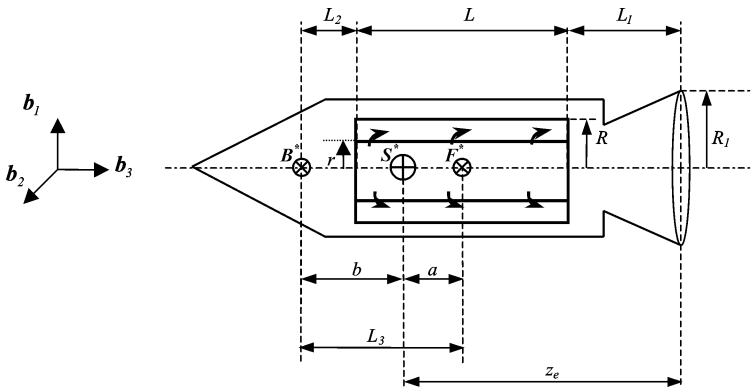

Figure 3.2. Rocket with propellant in centripetal burn.

where the subscripts B and F refer to bodies B and F respectively of Figure 2.1. Hence,

$$\bar{J}' = \bar{J}'_F = -\frac{1}{2}. \tag{27}$$

Substituting (23) and (27) into (13), we get

$$\psi(\tau) = -\frac{1}{2}(1-\beta^2). \tag{28}$$

From (28), $\psi(\tau)$ is a constant that can be negative, zero, or positive depending on the value of the nozzle expansion ratio β. There is thus a threshold value $\beta = \beta_L = 1$ for which the spin rate remains constant throughout the burn. The spin rate increases from ignition to burnout if $\beta > \beta_L$, and decreases from ignition to burnout for $\beta < \beta_L$. From (12), (26) and (28), a closed form solution can be shown to be

$$\frac{\bar{\omega}_3(\tau)}{\bar{\omega}_3(0)} = \left[\frac{2\bar{J}_B + 1}{2\bar{J}_B + 1 - \tau}\right]^{[1-\beta^2]}. \tag{29}$$

This expression confirms the above predictions.

3.2 Centripetal Burn

In centripetal burn, the cylindrical solid fuel is ignited at its periphery but not at any of its ends. It then burns radially inwards, with the radius decreasing uniformly along its length in such a way that the intermediate shape of the propellant is always a solid cylinder that has the same length as at ignition, but of decreasing radius (see Figure 3.2).

The mass of F at ignition remains as given by (18), and the intermediate mass of F during the burn is

$$m_F = \rho_{FO}\pi L r^2, \tag{30}$$

where r is the intermediate value of the external radius of the propellant. The time from ignition to burnout in this case is

$$t_b = \frac{m_{FO}}{-\dot{m}_F} = \frac{\rho_{FO}\pi L R^2}{-\rho_{FO}\pi L \frac{d}{dt}(r^2)} = \frac{R^2}{-\frac{d}{dt}(r^2)}. \tag{31}$$

This leads to

$$\left(\frac{r}{R}\right)^2 = 1 - \tau. \tag{32}$$

The dimensionless mass of the fuel is

$$\bar{m}_F = \frac{m_F}{m_{FO}} = \frac{\rho_{FO}\pi L r^2}{\rho_{FO}\pi L R^2} = \left(\frac{r}{R}\right)^2 = 1 - \tau \tag{33}$$

and once more,

$$\bar{m}' = \bar{m}'_F = -1. \tag{34}$$

The axial moment of inertia for the propellant is

$$J_F = \frac{m_F r^2}{2}. \tag{35}$$

So,

$$\bar{J}_F = \frac{J_F}{m_{FO}R^2} = \frac{\bar{m}_F}{2}\left(\frac{r}{R}\right)^2 = \frac{(1-\tau)^2}{2}. \tag{36}$$

For the overall system, we have

$$\bar{J} = \bar{J}_B + \bar{J}_F = \bar{J}_B + \frac{(1-\tau)^2}{2}. \tag{37}$$

Thus

$$\bar{J}' = \bar{J}'_F = -(1-\tau). \tag{38}$$

We then substitute (34) and (38) into (13) to obtain

$$\psi(\tau) = \left(\frac{\beta^2}{2} - 1\right) + \tau. \tag{39}$$

Equation (39) indicates that the function $\psi(\tau)$ increases linearly with time with unit slope, and $\psi(1) = \beta^2/2$ is greater than $\psi(0) = \beta^2/2 - 1$. $\psi(1)$ is always positive; however, $\psi(0)$ can be negative, zero, or positive depending on the value of β. Figure 3.3 captures the three possibilities. If the nozzle expansion ratio is equal to or greater than $\beta_L = \sqrt{2}$, the spin rate will decrease from ignition all the way to burnout. Otherwise, the spin rate increases initially, changes sign at some point during the burn, then decreases for the remainder of the burn. The trend reversal occurs at

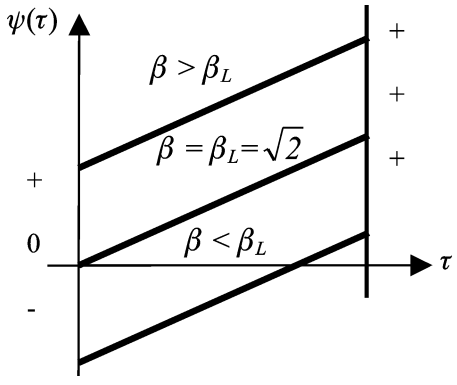

Figure 3.3. Function ψ for centripetal burn.

$$\tau = 1 - \beta^2/2. \tag{40}$$

A closed form solution is also possible for (12) in this case. Using (12), (37) and (39) we obtain

$$\frac{\bar{\omega}_3(\tau)}{\bar{\omega}_3(0)} = \left[\frac{2\bar{J}_B + 1}{2\bar{J}_B + (1-\tau)^2}\right] \cdot \exp\left\{\frac{-\beta^2}{\sqrt{2\bar{J}_B}}\left[\tan^{-1}\frac{\tau\sqrt{2\bar{J}_B}}{2\bar{J}_B + 1 - \tau}\right]\right\}. \tag{41}$$

Figure 3.4 shows plots of the normalized spin rate as a function of τ. The figure confirms the inferences given above.

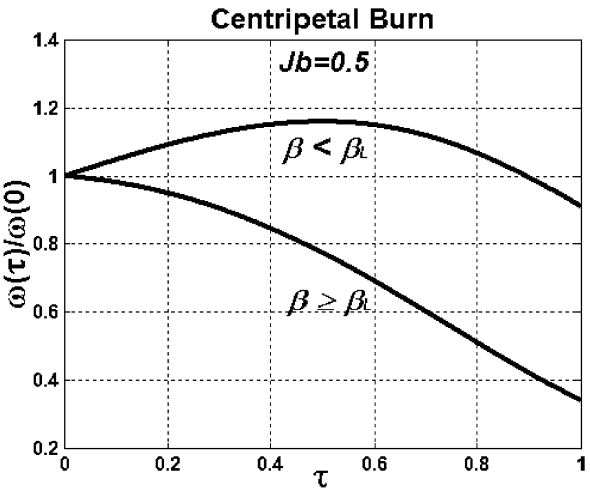

Figure 3.4. Spin behavior for centripetal burn.

3.3 Radial Burn

For radial burn, the cylindrical propellant is ignited along its axis, and burns radially outwards in such a way that the intermediate shape of the propellant is a hollow cylinder, as shown in Figure 3.5. This case was studied in detail in [6], but the highlights will be presented here for completeness.

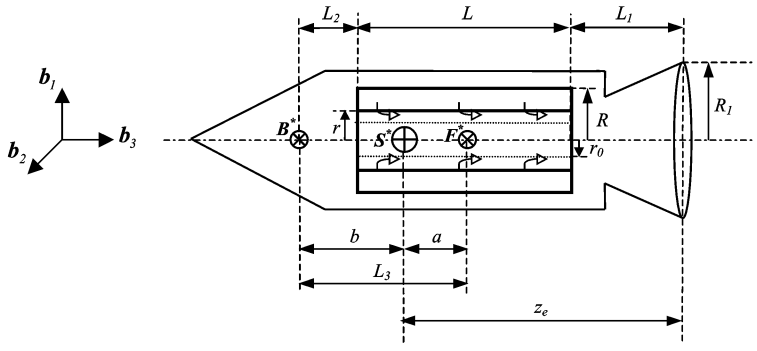

Figure 3.5. Rocket with radially burning propellant.

From Figure 3.5, the mass of propellant before ignition is

$$m_{F_O} = \rho_{FO}\pi L(R^2 - r_0^2) \tag{42}$$

and the propellant mass at some instant after ignition is

$$m_F = \rho_{FO}\pi L(R^2 - r^2). \tag{43}$$

In (42), r_0 is the internal radius of the propellant at ignition. The time from ignition to burnout is thus

$$t_b = \frac{m_{FO}}{-\dot{m}_F} = \frac{\rho_{FO}\pi L(R^2 - r_0^2)}{\rho_{FO}\pi L\,\frac{d}{dt}(r^2)} = \frac{R^2 - r_0^2}{\frac{d}{dt}(r^2)}. \tag{44}$$

Equation (44) can be integrated to give

$$\left(\frac{r}{R}\right)^2 = \left(\frac{r_0}{R}\right)^2 + \left[1 - \left(\frac{r_0}{R}\right)^2\right]\tau = \gamma^2 + (1-\gamma^2)\tau, \tag{45}$$

where γ is the ratio r_0/R. We get from (42) and (43)

$$\bar{m}_F = \frac{m_F}{m_{FO}} = \frac{\rho_F\pi L(R^2 - r^2)}{\rho_F\pi L(R^2 - r_0^2)} = \frac{1 - (r/R)^2}{1 - (r_0/R)^2} = 1 - \tau \tag{46}$$

and

$$\bar{m}' = \bar{m}'_F = -1. \tag{47}$$

The axial inertia of F is

$$\bar{J}_F = \frac{J_F}{m_{FO}R^2} = \frac{\bar{m}_F}{2}\left[1 + \left(\frac{r}{R}\right)^2\right] = \left[\frac{1-\tau}{2}\right][1 + \gamma^2 + (1-\gamma^2)\tau] \tag{48}$$

and that of the entire system is

$$\bar{J} = \bar{J}_B + \bar{J}_F = \bar{J}_B + \frac{1+\gamma^2}{2} - \gamma^2\tau - \frac{1-\gamma^2}{2}\,\tau^2. \tag{49}$$

Thus,

$$\bar{J}' = \bar{J}'_F = -[\gamma^2 + (1-\gamma^2)\tau]. \tag{50}$$

Equations (13), (47), and (50) give

$$\psi(\tau) = \left(\frac{\beta^2}{2} - \gamma^2\right) - (1-\gamma^2)\tau. \tag{51}$$

This time the function $\psi(\tau)$ varies linearly with τ, and has a slope of $(\gamma^2 - 1)$. The quantity $\gamma = r_0/R$ is strictly less than 1; hence, $\psi(\tau)$ has a negative slope. At ignition, $\psi(0) = (\beta^2/2 - \gamma^2)$, and this is likely to be positive for real rockets. At burnout, $\psi(1) = (\beta^2/2 - 1)$. Hence, when $\beta \geq \beta_L = \sqrt{2}$, the spin rate decreases all the way to burnout, and when $\beta < \beta_L$, the spin rate decreases at first, but then reaches a minimum value when $\tau = (\beta^2/2 - \gamma^2)/(1-\gamma^2)$, and starts to increase all the way to burnout.

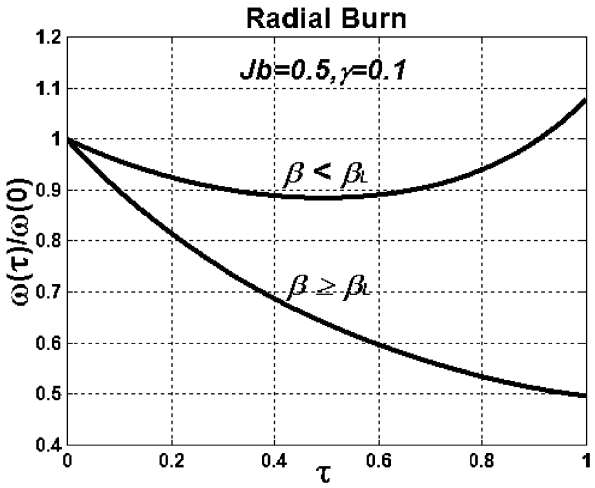

Figure 3.6. Spin rate behavior of radial burn.

Using equations (12), (49), and (51), it is again possible to solve for the spin rate in closed form:

$$\frac{\bar{\omega}_3(\tau)}{\bar{\omega}_3(0)} = \left[\frac{2\bar{J}_B(1-\gamma^2)+1-\gamma^4}{2\bar{J}_B(1-\gamma^2)+1-\left[\gamma^2+(1-\gamma^2)\tau\right]^2}\right] \tag{52}$$

$$\times \exp\left\{\frac{-\beta^2}{\sqrt{2\bar{J}_B(1-\gamma^2)+1}}\left[\tanh^{-1}\frac{\left[\gamma^2+(1-\gamma^2)\tau\right]}{\sqrt{2\bar{J}_B(1-\gamma^2)+1}} - \tanh^{-1}\frac{\gamma^2}{\sqrt{2\bar{J}_B(1-\gamma^2)+1}}\right]\right\}.$$

Figure 3.6 shows two cases that match the above predictions when $\bar{J}_B = 0.5$ and $\gamma = 0.1$ are used as an example.

4 Transverse Angular Speed

The magnitude of the transverse angular velocity is obtainable from (15), and is

$$\left|\frac{\bar{\omega}_T(\tau)}{\bar{\omega}_T(0)}\right| = \exp\left[-\int_0^\tau \frac{\varphi(\tau)}{\bar{I}}\,d\tau\right]. \tag{53}$$

The quantity $\bar{I}$ decreases with τ during a propellant burn, but is always positive. Hence, the sign of $\varphi(\tau)$ determines whether the magnitude of the transverse angular velocity increases or decreases with the burn. The central transverse moment of inertia of the rocket system can be written, in non-dimensional form as

$$\bar{I} = \bar{I}_B + \bar{I}_F + \frac{m_B b^2 + m_F a^2}{m_{FO} R^2}, \tag{54}$$

where the dimensionless transverse inertia of B is $\bar{I}_B = I_B/m_{FO}R^2$.

4.1 End Burn

For the case of End Burn [see Figure 3.1], the transverse inertia of the propellant F is

$$\bar{I}_F = \frac{I_F}{m_{FO}R^2} = \bar{m}_F\left[\frac{1}{4} + \frac{1}{12}\left(\frac{z}{R}\right)^2\right] = (1-\tau)\left[\frac{1}{4} + \frac{1}{12}\,\delta^2(1-\tau)^2\right], \tag{55}$$

where δ is the ratio L/R, which can be referred to as the shape factor of the solid propellant. In subsequent equations, we will use $\delta_i = L_i/R$, for $i = 1, 2, 3$ (see Figure 3.1 for L_1, L_2, L_3). The distances a and b can be expressed as

$$a = \frac{m_B}{m_B + m_F}\left[L_2 + \frac{L(1-\tau)}{2}\right] \tag{56}$$

and

$$b = \frac{m_F}{m_B + m_F}\left[L_2 + \frac{L(1-\tau)}{2}\right]. \tag{57}$$

Substituting equations (55), (56), and (57) into (54), and simplifying, we obtain

$$\bar{I} = \bar{I}_B + (1-\tau)\left[\frac{1}{4} + \frac{\delta^2(1-\tau)^2}{12}\right] + \frac{\bar{m}_B(1-\tau)}{\bar{m}_B + 1 - \tau}\left[\delta_2 + \frac{\delta(1-\tau)}{2}\right]^2. \tag{58}$$

Hence,

$$\bar{I}' = \left[\frac{1}{4} + \frac{\delta^2(1-\tau)^2}{4}\right] - \left[\frac{\bar{m}_B}{\bar{m}_B + 1 - \tau}\right]^2\left[\delta_2 + \frac{\delta(1-\tau)}{2}\right]^2 - \left[\frac{\bar{m}_B(1-\tau)\delta}{\bar{m}_B + 1 - \tau}\right]\left[\delta_2 + \frac{\delta(1-\tau)}{2}\right]. \tag{59}$$

Again from Figure 3.1, the distance

$$z_e = L_1 + L + a - \frac{z}{2}. \tag{60}$$

Thus

$$\frac{z_e}{R} = \frac{\bar{m}_B[\delta_2 + \delta(1-\tau)/2] + (\bar{m}_B + 1 - \tau)[\delta_1 + \delta(1+\tau)/2]}{\bar{m}_B + 1 - \tau}. \tag{61}$$

Finally, from (16), (23), (59), and (61), we get

$$\varphi(\tau) = -\frac{1}{4} + \frac{\beta^2}{4} + \delta_1^2 + \delta^2\tau + \delta\delta_1(1+\tau) + \frac{2\bar{m}_B[\delta_1 + \delta\tau]}{\bar{m}_B + 1 - \tau}\left[\delta_2 + \frac{\delta(1-\tau)}{2}\right] = -\frac{1}{4} + \varphi_e(\tau), \tag{62}$$

where

$$\varphi_e(\tau) = \frac{\beta^2}{4} + \delta_1^2 + \delta^2\tau + \delta\delta_1(1+\tau) + \frac{2\bar{m}_B[\delta_1 + \delta\tau]}{\bar{m}_B + 1 - \tau}\left[\delta_2 + \frac{\delta(1-\tau)}{2}\right]. \tag{63}$$

Since each parameter that appears in $\varphi(\tau)$ is positive, and $0 \le \tau \le 1$, it is clear that φ_e is always positive. In fact, it is most likely greater than $\frac{1}{4}$. Hence the function $\varphi(\tau)$ is likely to be always positive. We conclude then that in the case of End Burn, the

magnitude of the transverse angular velocity is damped as the propellant burns. The term "jet damping" truly applies in this case.

4.2 Centripetal Burn

We now consider the case of Centripetal Burn [see Figure 3.2]. Here,

$$\bar{I}_F = \frac{I_F}{m_{FO}R^2} = \bar{m}_F\left[\frac{1}{4}\left(\frac{r}{R}\right)^2 + \frac{1}{12}\left(\frac{L}{R}\right)^2\right] = (1-\tau)\left[\frac{1-\tau}{4} + \frac{1}{12}\,\delta^2\right], \tag{64}$$

$$a = \frac{m_B L_3}{m_B + m_F} \tag{65}$$

and

$$b = \frac{m_F L_3}{m_B + m_F}. \tag{66}$$

Substituting equations (64), (65), and (66) into (54), we obtain,

$$\bar{I} = \bar{I}_B + (1-\tau)\left[\frac{1-\tau}{4} + \frac{\delta^2}{12}\right] + \frac{\bar{m}_B(1-\tau)\delta_3^2}{\bar{m}_B + 1 - \tau} \tag{67}$$

so that

$$\bar{I}' = -\left(\frac{1-\tau}{2} + \frac{\delta^2}{12}\right) - \left(\frac{\bar{m}_B\delta_3}{\bar{m}_B + 1 - \tau}\right)^2. \tag{68}$$

In this case [see Figure 3.2],

$$z_e = L_1 + \frac{L}{2} + a. \tag{69}$$

So,

$$\frac{z_e}{R} = \frac{\bar{m}_B\delta_3 + (\bar{m}_B + 1 - \tau)(\delta_1 + \delta/2)}{\bar{m}_B + 1 - \tau}. \tag{70}$$

From equations (16), (34), (68), and (70)

$$\varphi(\tau) = -\frac{1}{2} + \frac{\tau}{2} + \frac{\beta^2}{4} + \frac{\delta^2}{6} + \delta_1^2 + \delta\delta_1 + \frac{\bar{m}_B\delta_3}{\bar{m}_B + 1 - \tau}\,(\delta + 2\delta_1) = -\frac{1}{2} + \varphi_c(\tau), \tag{71}$$

where

$$\varphi_c(\tau) = \frac{\tau}{2} + \frac{\beta^2}{4} + \frac{\delta^2}{6} + \delta_1^2 + \delta\delta_1 + \frac{\bar{m}_B\delta_3}{\bar{m}_B + 1 - \tau}\,(\delta + 2\delta_1). \tag{72}$$

We have here a situation that is similar to the End Burn case. $\varphi_c(\tau)$ is positive and increases with τ. $\varphi_c(\tau)$ is most likely greater than $\frac{1}{2}$, even at $\tau = 0$. Therefore the transverse angular speed is again a decreasing function from ignition to burnout.

4.3 Radial Burn

If the propellant undergoes a radial burn as shown in Figure 3.5,

$$\begin{aligned}\bar{I}_F = \frac{I_F}{m_{FO}R^2} &= \bar{m}_F\left[\frac{1}{4} + \frac{1}{4}\left(\frac{r}{R}\right)^2 + \frac{1}{12}\left(\frac{L}{R}\right)^2\right] \\ &= (1-\tau)\left[\frac{1 + \gamma^2 + (1-\gamma^2)\tau}{4} + \frac{\delta^2}{12}\right].\end{aligned} \tag{73}$$

The distances a and b become

$$a = \frac{m_B L_3}{m_B + m_F} \tag{74}$$

and

$$b = \frac{m_F L_3}{m_B + m_F}. \tag{75}$$

Substituting equations (73), (74), and (75) into (54), we obtain, after some algebra,

$$\bar{I} = \bar{I}_B + (1-\tau)\left[\frac{1+\gamma^2+(1-\gamma^2)\tau}{4} + \frac{\delta^2}{12}\right] + \frac{\bar{m}_B(1-\tau)\delta_3^2}{\bar{m}_B + 1 - \tau} \tag{76}$$

so that

$$\bar{I}' = -\left[\frac{\gamma^2+(1-\gamma^2)\tau}{2} + \frac{\delta^2}{12}\right] - \left[\frac{\bar{m}_B\delta_3}{\bar{m}_B + 1 - \tau}\right]^2. \tag{77}$$

Since, the distance

$$z_e = L_1 + \frac{L}{2} + a. \tag{78}$$

We have,

$$\frac{z_e}{R} = \frac{\bar{m}_B\delta_3 + (\bar{m}_B + 1 - \tau)(\delta_1 + \delta/2)}{\bar{m}_B + 1 - \tau}. \tag{79}$$

From equations (16), (47), (77), and (79)

$$\begin{aligned}\varphi(\tau) &= -\left[\frac{\gamma^2+(1-\gamma^2)\tau}{2}\right] + \frac{\beta^2}{4} + \frac{\delta^2}{6} + \delta_1^2 + \delta\delta_1 + \frac{\bar{m}_B\delta_3}{\bar{m}_B + 1 - \tau}(\delta + 2\delta_1) \\ &= \varphi_1(\tau) + \varphi_2(\tau),\end{aligned} \tag{80}$$

where

$$\varphi_1(\tau) = -\left[\frac{\gamma^2+(1-\gamma^2)\tau}{2}\right] \tag{81}$$

and

$$\varphi_2(\tau) = \frac{\beta^2}{4} + \frac{\delta^2}{6} + \delta_1^2 + \delta\delta_1 + \frac{\bar{m}_B\delta_3}{\bar{m}_B + 1 - \tau}(\delta + 2\delta_1). \tag{82}$$

Here, the minimum value that φ_1 can have is $-\frac{1}{2}$, but φ_2 is always positive and most likely greater than $\frac{1}{2}$. Hence, we have again that mass loss through radial propellant burn results in continuous damping of the transverse rate.

In summary, we find that the transverse angular velocity decreases in magnitude as propellant burn progresses for each of the three propellant-burn scenarios examined. We note, however, that this conclusion is not absolute. In other words, one cannot absolutely exclude the possibility of growth in the transverse angular speed with propellant burn. Some factors that could bring this about include small values of β, δ, δ_1, δ_2 and δ_3. We note that in [2] a variable mass cylinder model was used to show that the transverse rate can grow without bounds when the system is "short and fat," that is, for small δ. This makes sense because when a cylinder is used to model a rocket system, we automatically have that δ_i $(i = 1, 2, 3)$ are all zero and $\beta = 1$. If δ is small in addition, then there is a clear danger of having $|\varphi_2| < |\varphi_1|$ in (80). We also note that even for the extreme case of the cylinder, the authors [2] were not able to show divergence in transverse rate for End

and Centripetal Burns. It is easy to see this by setting $\delta_i = 0$ and $\beta = 1$ in equations (62) and (71).

5 Conclusion

This study examines how a spinning solid rocket's propellant depletion scheme affects the rotational dynamics of the rocket. Three mass loss scenarios – end burn, centripetal burn, and radial burn – were evaluated.

Results obtained indicate that for End Burn, spin rate can remain constant, increase, or decrease throughout the propellant burn depending on the value of the nozzle expansion ratio used. For Centripetal Burn, the spin rate will either decrease through the burn or increase at first then reverse itself and decrease to the end of the burn. In the case of Radial burn, the spin rate initially decreases then it can either keep decreasing or start increasing through the end of the burn. The value of the nozzle expansion ratio plays an important role in determining the character of the spin rate curve.

The transverse angular speed normally decreases with propellant burn irrespective of the type of burn adopted. For certain extreme choices of the parameters of the system, it may be possible to have the transverse rate increase with time for the radial burn.

References

[1] Eke, F.O. and Wang, S.M. Equations of motion of two-phase variable mass systems with solid base. *Journal of Applied Mechanics* **61**(4) (1994) 855–860.

[2] Eke, F.O. and Wang, S.M. Attitude behavior of a variable mass cylinder. *ASME Journal of Applied Mechanics* **62**(4) (1995) 935–940.

[3] Mao, T.C. and Eke, F.O. Attitude dynamics of a torque-free variable mass cylindrical body. *The Journal of the Astronautical Sciences* **48**(4) (2000) 435–448.

[4] Meirovitch, L. General motion of a variable mass flexible rocket with internal flow. *Journal of Spacecraft and Rockets* **7**(2) (1970) 186–195.

[5] Thomson, W.T. Equations of motion for the variable mass system. *AIAA Journal* **4**(4) (1966) 766–768.

[6] Sookgaew, J. and Eke, F.O. Effects of substantial mass loss on the attitude motions of a rocket-type variable mass system. *Nonlinear Dynamics and Systems Theory* **4**(1) (2004) 73–88.